Ply-overlap technique for joining dissimilar/hybrid composite materials

Jasim Ahamed[a], Mathew Joosten[a], Paul Callus[b], Michael R. Wisnom[c], and Chun H. Wang[a,*]

[a] Sir Lawrence Wackett Aerospace Research Centre, School of Engineering, RMIT University, GPO Box 2476, Melbourne VIC 3001 Australia

[b] Aerospace Division, DST Group, Melbourne, Australia

[c] Advanced Composites Centre for Innovation and Science, University of Bristol, Queen's Building, University Walk, BS8 1TR , Bristol, UK

Abstract

Hybridisation of multiple materials is emerging as a key strategy to achieving high performance lightweight structures while keeping the cost low. Fundamental to creating strong and cost-effective hybrid composites is the ability to efficiently join dissimilar materials. Herein we present a novel co-curing ply-overlap joint technique for integrating dissimilar composite materials. Experimental studies are conducted to identify the dominant failure mechanisms and the effect of design parameters, such as the spatial distances between ply terminations and overlap length, on the strength of hybrid composite ply-overlap joints. To enable optimisation of ply-overlap joints, analytical and computational models are developed and validated against the experimental data. The results demonstrate that ply-overlap joints are capable of approaching the un-notched strength of the glass composite material. The validated predictive tools enable design optimisation of hybrid composite structures.

Keywords: A. Hybrid B. Joint C. Strength D. Computational Modelling E. Multifunctional

1. Introduction

Integration of multiple materials enhances design flexibility and enables the optimal utilisation of materials with different properties to create affordable high-performance structures meeting diverse functional requirements [1]. Most common examples of such multi-material hybrid structures combine metals with advanced composite materials and can be found in large aircraft structural assemblies [2], ship hulls [3], automotive drive shafts [4] and bridge decks [5]. Hybrid structures combining dissimilar composite materials are also required for both structural and non-structural functions. For example, structural repair of a composite structure may be conducted with another composite material of

dissimilar stiffness and strength [6]. Another application which requires joints between dissimilar composites is multifunctional carbon fibre-reinforced plastic (CFRP) aircraft skin structures with an electrically insulating (dielectric) window fabricated from dielectric composites such as glass fibre reinforced plastic (GFRP) or quartz fibre reinforced Plastic (QFRP) to allow the transmission and reception of radiofrequency signals [7-9]. Fig. 1 shows an example of such multifunctional load-bearing antenna structure. One simple design approach is to assume that the dielectric window (denoted as radar transparent window in Fig. 1) does not carry any load and is treated as an open hole. In applications where the dielectric window is larger than the typical 6.35 mm diameter open hole used in aerospace design, significant local reinforcement around the dielectric window is required to ensure the structure can sustain the design loads. For example, the size of a half-wavelength slot antenna for X-band (8-12 GHz) applications ranges between 18.75 mm and 12.5 mm. The residual strength of an open hole within this size range will be substantially less than that pertinent to 6.35 mm diameter hole; therefore the aperture will need to be stiffened to meet the design ultimate strength requirement. This additional reinforcement around the dielectric window may be reduced, or eliminated entirely, by forming a co-cured hybrid joint of sufficient strength to carry the design loads.

Joining dissimilar composite materials requires careful design to maximise joint strength as the differing thermal and mechanical properties can affect the load carrying capacity of the joint. Co-curing is preferred over mechanical fastening or post-cure adhesive bonding for joining dissimilar composites as they offer higher structural efficiency and lower manufacturing cost. A number of co-cured ply joining techniques have been proposed in the literature [10] [11-13] [14] [15].The simplest technique is to butt individual plies by intelligently tailoring the positions of the ply terminations. Baucom *et al* [10] investigated several ply joining techniques for unidirectional CFRP laminates and found that the spatial distribution of ply terminations and the distance between adjacent ply terminations had a significant influence on the joint strength. Similar techniques were employed to efficiently transition from hybrid CFRP/titanium laminate to CFRP laminate for bolted joint applications [11-13]. For the load-bearing antenna applications, it is necessary to terminate all conductive CFRP plies outside the dielectric window for antenna requirements. Moreover, the introduction of a butted ply termination reduces the laminate strength by 35% [14]. The strength of an interleaved scarf joint, where the ply terminations are aligned along a linear scarf, between carbon fibre laminate and glass fibre laminate was found to be 31% lower than the un-notched strength of the glass fibre composite [15].

The aim of the present work is to develop a new joining technique to achieve higher joint strengths than ply-interleaved joints that have been reported in the literature [16]. An example of the new joining technique, denoted as the ply-overlap joint, is shown in Fig. 1. It should be noted that this type of joint has been developed specifically for use with integrated load bearing antenna structures. The structural behaviour of a number of ply-overlap joints is evaluated experimentally. Both analytical and Finite Element models are employed to predict ultimate joint strength. The work presented herein is outlined as follows. Section 2 discusses the key joint design considerations and describes the ply-overlap joint configurations. Details of the experimental program including manufacturing and testing of representative joint specimens, and the test results are provided in Section 3. Two modelling techniques used to predict joint strength are described in Section 4: analytical pull-out models based on delamination fracture theory and Finite Element models employing cohesive damage mechanics. This is followed by a discussion of the key findings and application to load-bearing antennae in Section 5. The main conclusions of this study are summarised in the final section.

2. Joint design

2.1 Design considerations

The primary function of a joint is to transfer loads efficiently between the CFRP structural skin and the GFRP dielectric window. To avoid unnecessary structural reinforcement surrounding the dielectric window the joint strength must exceed the minimum of the design allowable strengths of the CFRP skin and the GFRP dielectric window.

Achieving maximum load transfer between the dissimilar composite plies requires careful determination of the various design parameters. For a generic hybrid composite construction composed of dispersed overlaps between carbon and glass plies (Fig.2), these parameters include the carbon and glass ply orientations (θ_i^c and θ_i^g) respectively, the overlap length (l_i), and the spatial distribution of the overlaps or joint geometry. The locations of resin pockets are denoted by x_i, with the subscript i corresponding to the ply index. The overall joint length, L, is a function of the overlap length and joint geometry. The taper angle of the overlap region can be kept constant provided the overlaps are offset as shown in Fig.2. The ply-overlap technique, however, produces an undesirable increase in laminate thickness in the joint region. Ideally the joint geometry should be designed to be symmetric and flush, if possible, in order to minimise bending when the structure is loaded under compression, which can lead to high peel stresses. In addition to the mechanical considerations, thermal residual stresses caused

by the different coefficients of thermal expansion of carbon and glass composites must also be accounted for in the design. The key design challenge is then to achieve strength equal to or greater than that the design allowable strength of GFRP laminate, which is typically the open hole tension or compression strength, while minimising joint length and overlap thickness.

2.2 Joint concepts

In the current study three ply-overlap design configurations are proposed for joining quasi-isotropic CFRP and GFRP laminates as shown in Fig.3. The simplest technique is to overlap every ply, with all plies being terminated at the same location as shown in Fig. 3(a). This design configuration, which will be referred to as *aligned-overlap*, requires the shortest joint length but produces an undesirable abrupt thickness change: the thickness of the overlapped region is equal to the sum of the thicknesses of the two laminates. Alternatively, the overlaps can be staggered analogous to a double scarf as shown in Fig. 3(b). The *staggered-overlap* joint requires a comparatively long joint length but the taper angles of the overlap region are minimised. The third configuration, shown in Fig.3(c), produces a flush joint which is designed by selectively overlapping the main load-bearing plies aligned with the loading direction, while terminating the same number of weaker off-angle plies outside the joint region. In the *flush-overlap* configuration shown in Fig.3(c) for a layup of $[45/0/-45/90]_{2s}$, the 0^o glass plies are overlapped with 0^o carbon plies and $\pm 45^o$ glass plies are simply abutted with the carbon plies. The weakest plies which are the 90^o plies are terminated away from the joint. This joint design has the additional benefit of being symmetric which will result in reduced interlaminar peel stresses compared with the aligned or staggered overlap joints. The flush ply-overlap joint will be the focus of further investigation and the non-flush designs used for comparison purposes. In particular, the effect of overlap length on the strength of the flush ply-overlap joint will be investigated using experimental and numerical methods.

3. Experiments and Results

3.1 Materials & Manufacturing

Hybrid ply-overlap joints were manufactured using unidirectional prepregs of carbon/epoxy (T700/VTM264) and glass/epoxy (E-Glass/MTM57). The elastic and thermal properties of the two materials, obtained from manufacturer's data sheets supplemented by additional tests are given in Table 1. The cured ply thicknesses of carbon and glass plies were 0.21 mm and 0.26 mm respectively.

Conventional hand lay-up technique was employed to fabricate the joint panels. The CFRP and GFRP laminates had the same stacking sequence of $[45/0/-45/90]_{2s}$. Prior to layup, the positions of the ply terminations were marked onto a template to assist in accurate positioning of the plies. Carbon and glass plies were cut from their respective prepregs and layup was prepared in accordance with required joint configuration shown in Fig.3. Debulking was performed every four plies to consolidate the lay-up. The lay-up was then vacuum bagged and cured in the autoclave for 1 hr at 120^{o}C and 620 kPa in accordance with the manufacturer's recommendation. Tensile test specimens, 300 mm long and 25 mm wide, were prepared in accordance with the ASTMD3039 standard [17]. To compare the joint strengths with the un-notched quasi-isotropic laminate strengths, CFRP and GFRP samples were also fabricated and tested. The test matrix is summarised in Table 2.

Typical optical images of the fabricated joints are shown in Fig.4, including aligned overlap (Fig.4(a)), staggered overlap (Fig.4(b)), and flush overlap (Fig.4(c)) configurations. The maximum joint thickness for both the aligned and staggered joint was the same. However, the aligned joint featured a steeper taper angle. There was an observable deviation in the position of ply terminations due to the manufacturing tolerances and movement of plies during consolidation and curing. A detail view of a typical resin pocket adjacent to a ply termination is shown in Fig. 4(d).

3.2 Testing

Tensile tests were conducted using an INSTRON 4465 load frame equipped with a 50 kN load cell. Schematics of the tension and compression test fixtures are shown in Fig.5. Tabs are added to the carbon fibre laminate end so that the two ends of the specimens are aligned. A constant cross-head speed of 1 mm/min was employed and the load-displacement response was recorded at a rate of 4 Hz. Compressive tests were performed using the NASA short block test fixture [18] in a MTS hydraulic load frame equipped with a 100 kN load cell.

Compression test specimens, 50 mm long and 25 mm wide, were bonded 'back-to-back' to prevent bending due to eccentricity caused by different laminate thicknesses between the glass and carbon fibre laminates. The A constant cross-head speed of 0.5 mm/min for compression was applied and the load-displacement response was recorded at a rate of 4 Hz.

A minimum of four replicates for each configuration was tested. Stresses were calculated using the cross-sectional area of the GFRP laminate. Fractographic analysis was conducted to identify the failure modes through visual observation aided by high-resolution optical images of tested specimens.

3.3 Results

Tension

Typical stress-displacement responses for each joint configuration are shown in Fig.6(a) for tension and Fig.6(b) for compression. The stress is calculated using the nominal thickness of the GFRP laminate. The test results indicate that the joints exhibited an approximately linear-elastic response apart from the initial slacking caused by the tightening of the grips. Significant audible cracking was heard during the test for all joints at approximately 60% of the ultimate strength although no discernible change in global stiffness was detected. Upon reaching ultimate strength, brittle failure was observed for all the joints tested. The average tensile strengths with their coefficients of variation for all joint configurations are given in Table 2.

Examples of fracture specimens of aligned and staggered ply-overlap joints are shown in Fig.7(a) and Fig.7(b), respectively. In addition to delaminations at the interface between carbon and glass plies, limited fracture of carbon fibre plies were also observed, likely due to the secondary bending caused by the steep tapering angles (Fig. 3). The fracture modes for flush joints of 3 mm and 6 mm overlap length were very similar, with delaminations between the carbon 0^o plies and glass 0^o plies emanating from the root of the overlap region being the principal failure mode. Fig.7(c-1) shows the typical fracture topography of flush joints with 6 mm overlap length. The delaminated plies were then isolated and observed under scanning electron microscopy (SEM) to determine the delamination crack path. For flush ply-overlap joint specimens with 9 mm step length, failure was observed in the GFRP laminate away from the joint region as shown in Fig.7(c-2). Failure in the glass laminate indicates that the joint strength is greater than the un-notched GFRP strength. Several carbon fibres remained bonded to the fracture surfaces of the glass plies, Fig.8 (a & b). Carbon fibres on the glass plies is indicative of the delamination crack propagating primarily within the carbon fibre plies adjacent to the glass laminate.

Compression

Stress-displacement responses for all four specimens demonstrated approximately linear elastic behaviour followed by catastrophic brittle failure, referring to Fig. 6(b). The failure modes and peak loads were fairly consistent for all but one test specimen that buckled due to failure of the adhesive used to bond the specimens. The average compression strength of the flush joints was measured to be 300±3 MPa, which is approximately 90% of the GFRP laminate compression strength (Table 2). Optical images shown in Fig. 9 indicate the typical fracture surface topography of the compression-tested joints. Delaminations can be seen in the joint region between the overlapped carbon and glass plies and in the GFRP laminate. The images also reveal some fractured 0^o glass plies and transverse matrix cracks in the off-axis ($\pm 45^o/90^o$) plies. Microbuckling of glass fibres may have occurred after delaminations. It has been reported that microbuckling occurs when steep taper angles are involved [19].

4. Analysis Methods

4.1 Analytical modelling

The principal failure mode of flush ply-overlap joints was pull-out of the carbon plies from the joint as schematically depicted in Fig.10(a). To predict the delamination strength, a limit strength analysis for joints with "short" overlaps as shown Fig.10(b) and a fracture mechanics approach for joints of "long" overlaps as shown in Fig.10(c) were developed. Details of the models are provided in the following sections. These analytical models build on the methods developed by the authors for unidirectional hybrid composite joints [15, 20] .

Short overlap

For short overlap lengths (relative to a critical load transfer length), the interlaminar shear stress between the overlapped plies is approximately constant within the overlap region. A short overlap joint therefore fails when the interlaminar stress exceeds the interlaminar shear strength of the matrix, similar to the limit analysis method for determining structural collapse loads. Due to the difference in laminate thickness of the two materials, peel stresses must be considered. Fig.10(a) schematically illustrates the interlaminar peel and shear stresses in a short overlap joint. The peel stress, σ_{33}, can be expressed in terms of the shear stress τ_{13} by appealing to the equilibrium condition,

$$\sigma_{33} = \tau_{13} \tan\alpha \quad (1)$$

where α is the average taper angle of the joint calculated using the two laminate thicknesses assuming linear change in thickness. At failure, the interlaminar shear and peel stresses obey the following quadratic failure criterion

$$\left(\frac{\tau_{13}}{S_{13}}\right)^2 + \left(\frac{\sigma_{33}}{S_{33}}\right)^2 = 1 \quad (2)$$

where S_{13} and S_{33} are the interlaminar shear and interlaminar peel strength of the composite ply.

From equilibrium condition, the applied stress is

$$\sigma_s = n\left(\frac{L}{T}\right)(\tau_{13}\cos\alpha + \sigma_{33}\sin\alpha) = n\left(\frac{L}{T}\right)\frac{\tau_{13}}{\cos\alpha} \quad (3)$$

where Eq.(1) has been used, T denotes the GFRP laminate thickness, and n denotes the number of debonding interface, assuming all the interfaces delaminate simultaneously. For the flush joint in this study, $n = 8$ since there are four carbon 0^o plies and debonding occurs on both sides of each ply. Therefore the interlaminar shear and peel stresses can be expressed in terms of the applied stress

$$\tau_{13} = \sigma_s \frac{T}{nL}\cos\alpha \quad (4)$$

$$\sigma_{33} = \sigma_s \frac{T}{nL}\sin\alpha \quad (5)$$

The pull-out strength σ_s can be determined by inserting Eq.(4) and Eq.(5) into Eq.(2), yielding

$$\sigma_s = \frac{nL}{T}\frac{1}{\sqrt{\left(\frac{\cos\alpha}{S_{13}}\right)^2 + \left(\frac{\sin\alpha}{S_{33}}\right)^2}} \quad (6)$$

where S_{13} and S_{33} are the interlaminar shear and interlaminar peel strength of the composite ply. Based on the fractographic observations that delamination occurs within the carbon ply at the interface, the appropriate values of S_{13} and S_{33} are those of CFRP listed in Table 4.

Long overlap

At long overlap lengths, the interlaminar shear stresses are zero almost everywhere in the interface, except at the ply termination where a stress singularity exists. Since the resin pockets have very low stiffness and strength (thus fracture well before the ultimate strength of the joint), they can be assumed to act as voided regions and the delamination strength can be determined by using the strain energy release rate (SERR) method.

The critical value of SERR required for the unstable growth of a delamination crack is equal to the rate of change in potential strain energy of the hybrid laminate or joint region shown in Fig. 10(c) before and after delamination. Under a constant applied load of N^{∞}, and assuming unit width, the energy balance equation can be written as follows:

$$2nG_C = -\frac{\left(\frac{N^{\infty}}{h_i}\right)^2}{2E_i} h_i + \frac{\left(\frac{N^{\infty}}{h_f}\right)^2}{2E_f} h_f \tag{7}$$

where E and h are the stiffness and the thickness of the hybrid laminate, with the subscripts i and f denoting pertinent values before and after delamination. Parameter n represents the number plies that disbond and G_C is the critical strain energy release rate. The factor of 2 on the left hand side of Eq.(4) is to account for fracture on both surfaces of a delaminating ply. Rearranging the terms in Eq. (4) yields the formula for the applied load to cause complete separation of the glass and carbon fibre laminates by delamination cracking,

$$N^{\infty} = \sqrt{\frac{4nG_C E_i E_f h_i h_f}{E_i h_i - E_f h_f}} \tag{8}$$

Under tensile loading, the delaminations are driven by the Mode II fracture toughness ($G_c = G_{IIc}$) because the peel stresses are compressive, except at the tip of the ply termination. Under compression loading, the peel stresses are tensile and therefore delamination is affected by the peeling mode. To account for this mixed-mode delamination in compression, we employ the B-K law [21] to calculate the mixed-mode fracture toughness

$$G_C = \begin{Bmatrix} G_{IIc} & \sigma_{33} \le 0 \\ G_{Ic} + (G_{IIc} - G_{Ic}) \left(\frac{G_{II}}{G_I + G_{II}}\right)^{\eta} & \sigma_{33} > 0 \end{Bmatrix} \tag{9}$$

where σ_{33} is the interlaminar peel stress at a ply thickness distance away from the ply termination and the mode-mixity ratio is estimated from the ratio of interlaminar shear and peel stresses at the same distance using linear finite element analysis. Using a value of η=2 [22] and mode-mix ratio of 0.58, obtained from linear FE analysis, the critical SERR for compression is 0.625 N/mm^2. Laminate stiffness values are determined used classical laminate theory and delamination stress is determined using Eq.(5) divided by the GFRP laminate thickness.

4.2 Numerical modelling

The creation and analysis of finite element models was conducted using commercially available finite element software, ABAQUS Explicit version 6.12 [23]. The geometry and mesh of the FE model for a flush ply-overlap joint of 9 mm overlap length is shown in Fig.11. The FE model consists of the joint region and a 25 mm length of the CFRP and GFRP laminate regions of the test specimen. The entire width (25 mm) of the test specimen was modelled. Plies in the overlap region were assumed to taper linearly from the nominal GFRP laminate thickness to the nominal CFRP laminate thickness. The sizes of the triangular and rectangular resin pockets were estimated from the micrographs of the specimens to be approximately 1 mm and 0.2 mm in length respectively. Using nominal ply thickness of GFRP (0.26 mm) the taper angle for the overlapped 0^o glass plies at the triangular resin pocket is determined to be 14.5^o. The joint geometry employed here assumes perfect alignment of the resin pockets. The effect of this geometric idealisation will be investigated later.

Each ply of the hybrid composite joint was discretised with eight node reduced integration continuum shell elements (SC8R) [23] while the resin pockets were discretised with eight node reduced integration continuum solid elements (C3D8R) [23]. Linear elastic behaviour was assigned to the plies while a stress-softening model was used to simulate the failure process of resin pockets. Cohesive elements [22, 24, 25] were inserted at every dissimilar interface in the joint region and extended to 3 mm in the laminates to capture the delamination damage. The dimensions of the cohesive element, 0.2 mm by 0.5 mm, were chosen based on the recommendations in [26, 27] to alleviate mesh dependence of the numerical results. The in-plane dimensions of the shell elements were identical to the cohesive elements. Each ply was discretised with three elements through the thickness to improve the bending response and capture the stress gradient near the resin pockets more accurately. The properties of the cohesive elements representing delamination within CFRP and GFRP laminates are listed in Table 4. The interlaminar strength and fracture toughness of carbon laminate were used for the cohesive elements between carbon-glass ply interfaces, based on the experimental observations that

delamination occurred primarily within the carbon laminate. The B-K law [21] was employed to simulate effect of mixed fracture mode. The CFRP laminate end of the model was fixed in all degrees of freedom and the GFRP laminate end was prescribed a displacement in the loading direction with other degrees of freedom fixed. Prior to the static analysis, a thermal analysis step was performed with $\Delta T = -100℃$ to account for the effect of residual thermal stresses and strains resulting from the cure.

Since fractographic evidence presented in previous section for compression experiments showed both delaminations and fibre fracture of glass plies, the ABAQUS progressive damage model [28] was used to simulate compressive fibre failure. The model requires the fibre fracture strength $X_{11,c}$ for damage initiation and fibre compressive fracture energy G_{fc} for damage propagation. The values of $X_{11,c} = 1000$ MPa and $G_{fc} = 40\ \mathrm{N/mm^2}$ were obtained from previous publications on the same material system [15, 20].

5. Analysis results

5.1 FE damage progression

Tension

The deformed states of the FE model at three stages damage onset, propagation and final failure for the ply-overlap joint under tensile loading is shown in Fig.12(a). The maximum interlaminar stress concentrations were adjacent to the terminations of off-axis glass plies, thereby, initiating damage between the G0^o-C0^o interfaces (here G and C denote glass and carbon fibre plies) at approximately 80% of the ultimate load, as shown in Fig.12(a). The delamination propagation was initially stable, i.e. a small increase in crack length with increasing load. Fatal delaminations that cause the separation of the glass and carbon laminates were at the interface between glass and carbon laminates, as shown in the first image of Fig.12(a).

Compression

Under compressive loading, delamination failure was observed to initiate in the G0^o-C0^o interfaces at a lower load due to the presence of tensile peel stresses, approximately 60% of the ultimate compression strength. The deformed states of the FE model showing the damage onset, propagation and final failure under compressive loading are presented in Fig.12(b). Delaminations were predicted

to occur within the GFRP laminate. The delamination grew in a stable manner initially until upon reaching a critical size and then propagaed unstably at the ultimate load.

5.2 Comparison of strength predictions with experiments

Comparison of strength predictions obtained from the analytical models and the FE model with the experiments are shown in Fig.13. The short overlap analytical model, Eq.(2), clearly overpredicts the experimental results as the assumptions are only valid for joints of very short overlap length. The long overlap analytical model, Eq.(5), based on fracture mechanics approach gives almost identical predictions as the FE model employing CZM for 9 mm flush joints. In compression, the anaytical approach was conservative as it underpredicted the joint strengths. This may be due the assumption of constant mode-mixity ratio which in reality may vary with delamination size. Overall, the FE model was capable of predicting the experimentally measured joint strengths. The effect of various parameters that influence the FE strength prediction are discussed below.

Thermal residual stresses

Comaprison of strength predictions for analysis with and without the effect of thermal residual stresses is shown in Table 4. Inclusion of the residual thermal stresses resulted in an increase in tensile strength of 7% and a reduction in compressive strength of 2.5% . This is expected as the thermal residual stress is small for balanced joints.

Effect of spatial distribution of ply termination

The computational modelling considers perfectly aligned geometry for the flush overlap joint. Manufacturing variations can however affect the positions of the overlaps which may in turn influence the joint strength. Two possible misaligned spatial distribution of critical ply terminations have been investigated: a symmetric offset configuration in which overlaps were offset by a fixed distance while retaining joint laminate symmetry as shown in Fig.14(a), and an asymmetric offset configuration in which overlaps are arbitarily dispersed as shown in Fig.14(b).

Comparison of the strength predictions of the baseline geometry (Fig.11) with the non-idealised configurations Fig.14(a) and Fig.14(b) are shown in Fig.15. The results indicate that employing a symmetric offset configuration increased the tensile and compressive strengths by 2%. The increase in strength is small because the strength critical ply terminations are several ply thicknesses away from

each other and therefore stress concentrations do not interact (or are "elastically isolated" as discussed in [29]). For the asymmetric configuration the predicted tensile strength was unaffected whilst the compressive strength reduced by 9%. This reduction in compressive strength can be attributed to the increased bending loads due to joint asymmetry that give rise to increasing detrimental peel stresses.

Effect of overlap length

FE models of different overlap lengths were used to predict joint strength versus overlap length with the results shown in Fig.13. The simplified analytical pull-out models are able to provide upper and lower strength limits, however, the FE model allows the intermediate region between short and long overlaps to be accurately predicted. The FE model demonstrates that there is a gradual increase in strength followed by the intermediate region where the gradient change in strength is much lower. Above a certain length, the joint strength increases by less than 1%. This critical joint length, commonly referred as the transfer length for adhesively bonded joints, is usually defined as the joint length at which 95% of the "maximum" load-carrying capacity of the joint is achieved [30]. Following this definition, the transfer length for the flush joint is estimated as 9 mm, referring to Fig.13(a), in tension and 6 mm in compression as shown in Fig.13(b).

6. Discussion

Experimental studies have shown that achieving high strength using the ply-overlap technique requires judicious selection of spatial distribution of ply terminations and overlap length. The highest coefficient of variation in strength results was found to be 5% which shows low sensitivity to manufacturing variations in ply-overlaps. For the overlap lengths investigated, the strength of flush joints increased steadily with overlap length. Failure of 9 mm overlap joint specimens in the GFRP laminate suggests that the strength of joint equals or exceeds the GFRP laminate strength. The flush joint design which overlaps only the main load-bearing plies outperforms the aligned and staggered joint designs as eccentric loading is minimised. However, the staggered joint may be preferred for implementation to 3D load-bearing antenna structure as the flush joint design will require non-circular/irregular shaped GFRP inserts. The staggered joint could be optimised by introducing mid-plane symmetry to the design thereby reducing the overall joint length. The required overlap length would be greater than the transfer length of 9 mm to account for manufacturing variations. In a load-bearing antenna structure which is composed of low stiffnesss (GFRP) insert surrounded by a high

stiffness material (CFRP), the joint will attract less load due to the load-shedding effect [31]. The reduction in load in the joint will further reduce the joint length.

Fractographic evidence indicated that the principal failure mode was delamination at the bi-material interface. Delamination occurred within the carbon laminate due its lower toughness than the glass laminate. Numerical models employing cohesive elements were able to accurately capture this delamination mode observed in the experiments and were shown to give excellent correlation with the ultimate strength. Future work will focus on incorporating damage models capable of modelling transverse matrix cracking which has been shown to be an important damage mechanism especially in compression [32-34].

The primary function of ply-overlap joints for load-bearing antennas is to allow for structural credit to be given to dielctric windows which are traditionally treated as open-holes. The dielectric window size is proptional to the operating frequency and therefore this joining technique is particulary important for moderate to low frequency, including the X-band (8-12 GHZ), applications. These techniques can also be extended to hybrid structural applications for which efficient methods are required to transition between two dissimilar composite laminates without needing additional reinforcements.

7. Conclusion

The structural behaviour of hybrid CFRP/GFRP ply-overlap joints has been investigated using experimental, analytical and numerical methods. The principal failure mode observed in the experiments was delamination emanating from ply terminations in the vicinity of the overlapped plies. Through judicious selection of the spatial distribution of ply terminations and overlap length, the ply-overlap joints can be designed to reach a strength approaching the un-notched GFRP laminate strength. A stacked shell modelling FE methodology has been found to accurately predict the delamination path and ultimate loads recorded during experimental testing. The validated FE modelling approach is a valuable design tool that can be used to efficiently design an integrated radar transparent window for load-bearing antenna applications using the ply overlapping technique. These new joining techniques provide effecient load transfer between two dissimilar composite laminates without needing additional reinforcements.

Acknowledgements

The author would also like to acknowledge DST-Group and DMTC members for their continued involvement in the project. Special thanks also to RMIT technical officers, Robert Ryan and Peter Thatchyk.

References

1. Zhang, J., et al., *Hybrid composite laminates reinforced with glass/carbon woven fabrics for lightweight load bearing structures.* Materials & Design, 2012. **36**: p. 75-80.

2. Hale, J., *Boeing 787 From Ground Up*, in *Boeing Commercial Aeromagazine*. 2012.

3. Matsuzaki, R., M. Shibata, and A. Todoroki, *Improving performance of GFRP/aluminum single lap joints using bolted/co-cured hybrid method.* Composites Part A: Applied Science and Manufacturing, 2008. **39**(2): p. 154-163.

4. Abu Talib, A.R., et al., *Developing a hybrid, carbon/glass fiber-reinforced, epoxy composite automotive drive shaft.* Materials & Design, 2010. **31**(1): p. 514-521.

5. Keller, T., E. Schaumann, and T. Vallée, *Flexural behavior of a hybrid FRP and lightweight concrete sandwich bridge deck.* Composites Part A: Applied Science and Manufacturing, 2007. **38**(3): p. 879-889.

6. Harman, A.B. and C.H. Wang, *Improved design methods for scarf repairs to highly strained composite aircraft structure.* Composite Structures, 2006. **75**(1-4): p. 132-144.

7. Callus, P.J., *Conformal Load-Bearing Antenna Strcuture for Australian Defence Force Aircraft*, A.V. Division, Editor. 2007.

8. Callus, P.J., *Novel concepts for Conformal Load-bearing Antenna Structure*, A.V. Division, Editor. 2007.

9. Callus, P.J., et al., *Slotted Waveguide Antenna Stiffened Structure* 2012. US Patent No. 8149177 B1

10. Baucom, J.N., et al., *Tiled Composite Laminates.* Journal of Composite Materials, 2010. **44**(26): p. 3115-3132.

11. Camanho, P.P., et al., *Hybrid titanium–CFRP laminates for high-performance bolted joints.* Composites Part A: Applied Science and Manufacturing, 2009. **40**(12): p. 1826-1837.

12. Fink, A., et al., *Hybrid CFRP/titanium bolted joints: Performance assessment and application to a spacecraft payload adaptor.* Composites Science and Technology, 2010. **70**(2): p. 305-317.

13. Kolesnikov, B., L. Herbeck, and A. Fink, *CFRP/titanium hybrid material for improving composite bolted joints.* Composite Structures, 2008. **83**(4): p. 368-380.

14. Malkin, R., et al., *Bio-inspired laminate design exhibiting pseudo-ductile (graceful) failure during flexural loading.* Composites Part A: Applied Science and Manufacturing, 2013. **54**: p. 107-116.

15. Ahamed, J., M.W. Joosten, and C.H. Wang, *Ply-interleaving Technique for Joining Hybrid Carbon/Glass Fibre Composite Materials.* Composites Part A: Applied Science and Manufacturing, 2016. **Accepted Manuscript**.

16. Ahamed, J., et al., *Ply-interleaving technique for joining hybrid carbon/glass fibre composite Materials* Composites Part A, 2016: p. (in press).

17. ASTM D3039 / D3039M-14, Standard Test Method for Tensile Properties of Polymer Matrix Composite Materials, International, A., West Conshohocken, PA, 2014

18. Shuart, M.J., *Failure of compression-loaded multidirectional composite laminates.* AIAA Journal, 1989. **27**(9): p. 1274-1279.

19. Steeves, C.A. and N.A. Fleck, *Compressive strength of composite laminates with terminated internal plies.* Composites Part A: Applied Science and Manufacturing, 2005. **36**(6): p. 798-805.

20. Ahamed, J., M. Joosten, and C.H. Wang, *Novel hybrid co-cured carbon / glass fibre composite joints for safety critical structures*, in *International Conference on Composite Materials(ICCM) 19*. 2015: Montreal. p. 19-24.

21. Benzeggagh, M.L. and M. Kenane, *Measurement of mixed-mode delamination fracture toughness of unidirectional glassepoxy composites with mixed.* Composites Science and Technology, 1996. **56**: p. 439-449.

22. Turon, A., et al., *Accurate simulation of delamination growth under mixed-mode loading using cohesive elements: Definition of interlaminar strengths and elastic stiffness.* Composite Structures, 2010. **92**(8): p. 1857-1864.

23. Dassault Systèmes Simulia Corp., P., RI, USA, *Abaqus 6.12*. 2012.

24. Turon, A., et al., *A damage model for the simulation of delamination in advanced composites under variable-mode loading.* Mechanics of Materials, 2006. **38**(11): p. 1072-1089.

25. Yang, Q. and B. Cox, *Cohesive models for damage evolution in laminated composites.* International Journal of Fracture, 2005. **133**(2): p. 107-137.

26. Harper, P.W. and S.R. Hallett, *Cohesive zone length in numerical simulations of composite delamination.* Engineering Fracture Mechanics, 2008. **75**(16): p. 4774-4792.

27. Turon, A., et al., *An engineering solution for mesh size effects in the simulation of delamination using cohesive zone models.* Engineering Fracture Mechanics, 2007. **74**(10): p. 1665-1682.

28. Lapczyk, I. and J.A. Hurtado, *Progressive damage modeling in fiber-reinforced materials.* Composites Part A: Applied Science and Manufacturing, 2007. **38**(11): p. 2333-2341.

29. Allegri, G., M.R. Wisnom, and S.R. Hallett, *A simplified approach to the damage tolerance design of asymmetric tapered laminates. Part II: Methodology validation.* Composites Part A: Applied Science and Manufacturing, 2010. **41**(10): p. 1395-1402.

30. Baker, A., S. Dutton, and D. Kelly, *Composite Materials for Aircraft Structures (2nd Edition)*. 2004, Reston,VA: American Institute of Aeronautics and Astronautics.

31. Rose, L.R.F., *An application of the inclusion analogy for bonded reinforcements.* International Journal of Solids and Structures, 1981. **17**(8): p. 827-838.

32. Lemanski, S.L., et al., *Modelling failure of composite specimens with defects under compression loading.* Composites Part A: Applied Science and Manufacturing, 2013. **48**: p. 26-36.

33. Mukhopadhyay, S., M.I. Jones, and S.R. Hallett, *Compressive failure of laminates containing an embedded wrinkle; experimental and numerical study.* Composites Part A: Applied Science and Manufacturing, 2015. **73**: p. 132-142.

34. Tsampas, S.A., et al., *Compressive failure of hybrid multidirectional fibre-reinforced composites.* Composites Part A: Applied Science and Manufacturing, 2015. **71**: p. 40-58.

Tables

Table 1 Ply elastic and thermal properties

	T700/VTM264 (CFRP)	E-glass/MTM57 (GFRP)
E_1 (MPa)	120200	34160
E_2, E_3 (MPa)	7467	7870
G_{12}, G_{13} (MPa)	3904	3700
G_{23} (MPa)	2304	3098
ν_{12}, ν_{13}	0.32	0.27
ν_{23}	0.33	0.27
α_{11} (10^{-6}/℃)	-0.3	6
α_{22} (10^{-6}/℃)	25	35

Table 2 Test Matrix

Test Method	Configuration	Overlap Length (mm)	Average strength (MPa)	Coefficient of variation (%)
Tension	Aligned	9	278	3
	Staggered	9	316	11.3
	Flush	3	302	3.8
	Flush	6	330	1.2
	Flush	9	354	0.2
	CFRP		833	3.5
	GFRP		354	5.7
Compression	Flush	9	300	1
	CFRP		520	1.7
	GFRP		331	5.1

Table 3 Interlaminar damage properties used for cohesive elements

	T700/VTM264	E-glass/MTM57
Interlaminar peel strength, S_{33} (MPa)	40*	47*
Interlaminar shear strength, S_{13} (MPa)	77*	78*
Interlaminar shear strength, S_{23} (MPa)	77 (Assumed equal to S_{13})	78 (Assumed equal to S_{13})
Mode I fracture toughness, G_{IC} (KJ/m^2)	0.3 *	0.4 *
Mode II fracture toughness, G_{IIC} (KJ/m^2)	1.6*	2.4*
Mode III fracture toughness, G_{IIIC} (KJ/m^2)	1.6 (Assumed equal to G_{IIc})	2.4 (Assumed equal to G_{IIc})
Cohesive stiffness, K_I, K_{II}, K_{III} (N/mm^3)	1×10^6 [22]	1×10^6 [22]

*Tested at RMIT

Table 4 Comparison of FE predictions with experimental results for flush ply-overlap joint

Test Method	Overlap Length (mm)	Experimental strength (MPa)	FE (CZM)	FE (CZM No thermal)
Tension	3	302±12	232	239
	6	330±4	344	372
	9	354±1	385	415
Compression	9	300±2.8	284	278

List of Figures

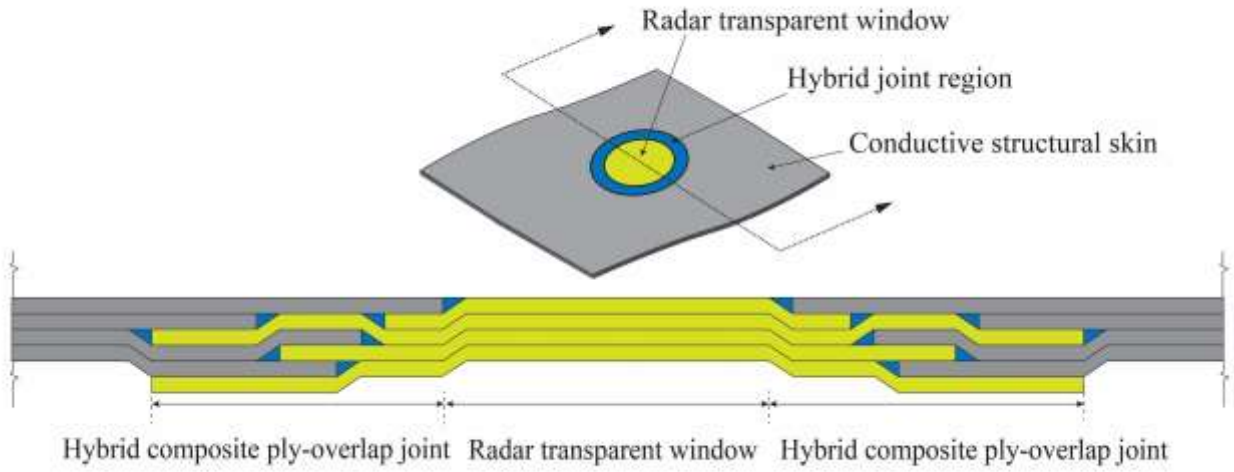

Fig. 1 Multifunctional load-bearing antenna structure using hybrid composite ply-overlap joint

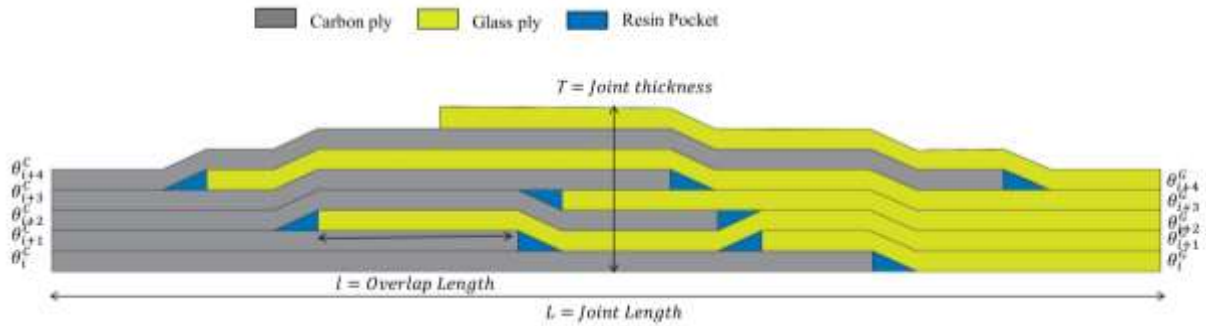

Fig. 2 Hybrid composite ply-overlap joint design parameters

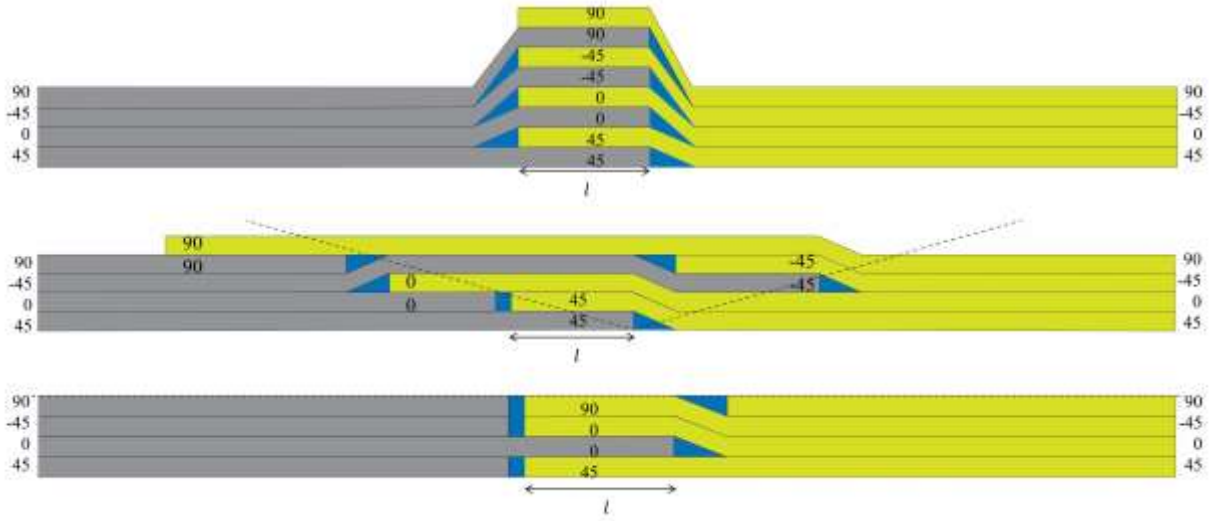

Fig. 3 Hybrid composite ply-overlap joint configurations (a) Aligned overlap (b) Staggered overlap and (c) Flush overlap

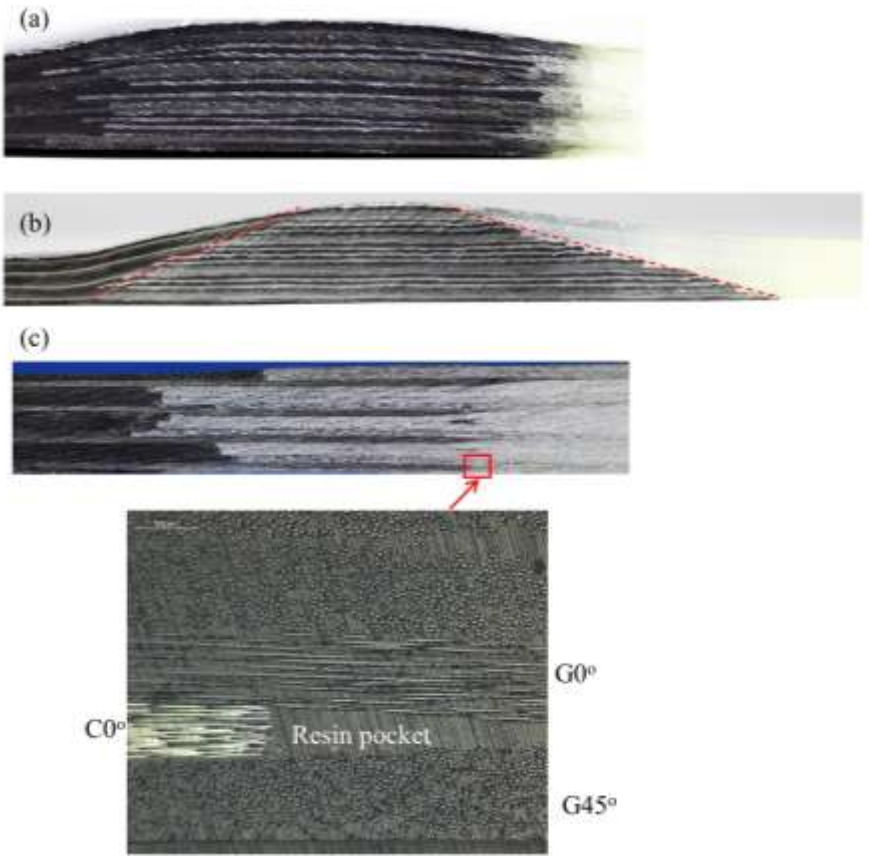

Fig.4 Optical images of fabricated joint specimens. (a) Aligned-overlap, (b) staggered-overlap, (c) flush-overlap and high resolution microscopic image of a typical resin-rich pocket at a ply termination.

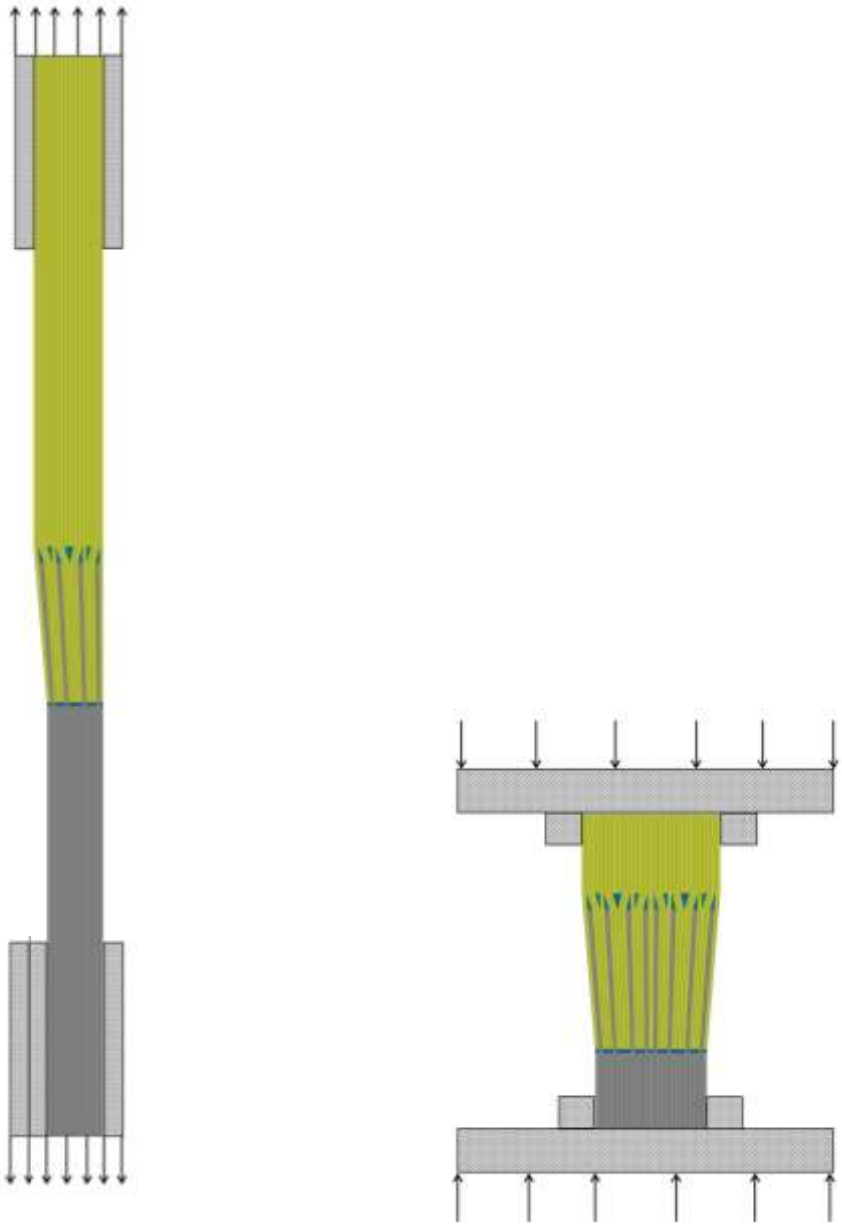

(a) (b)

Fig. 5 Test fixture (a) Tension (b) Compression

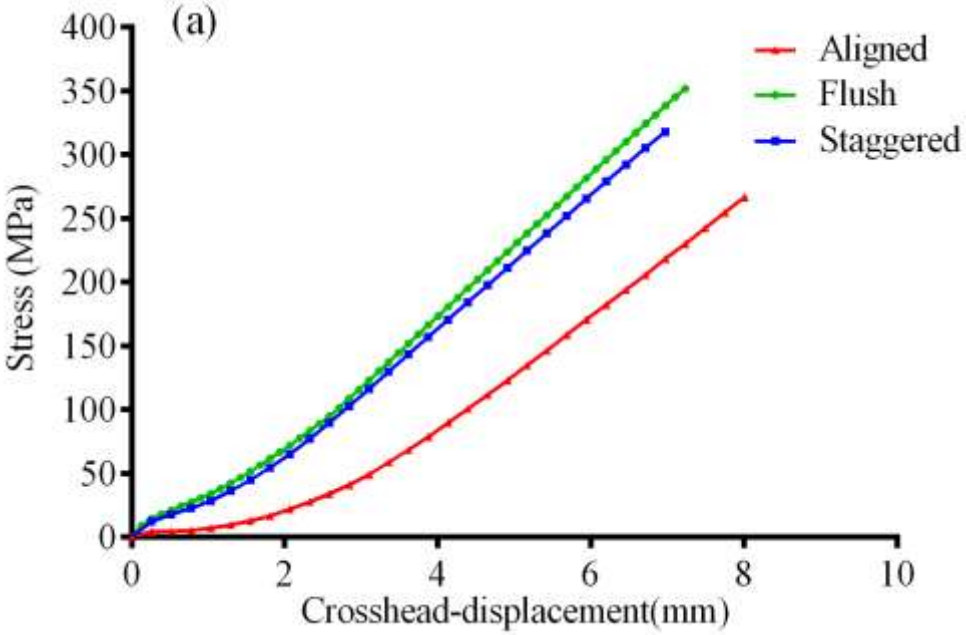

(a)

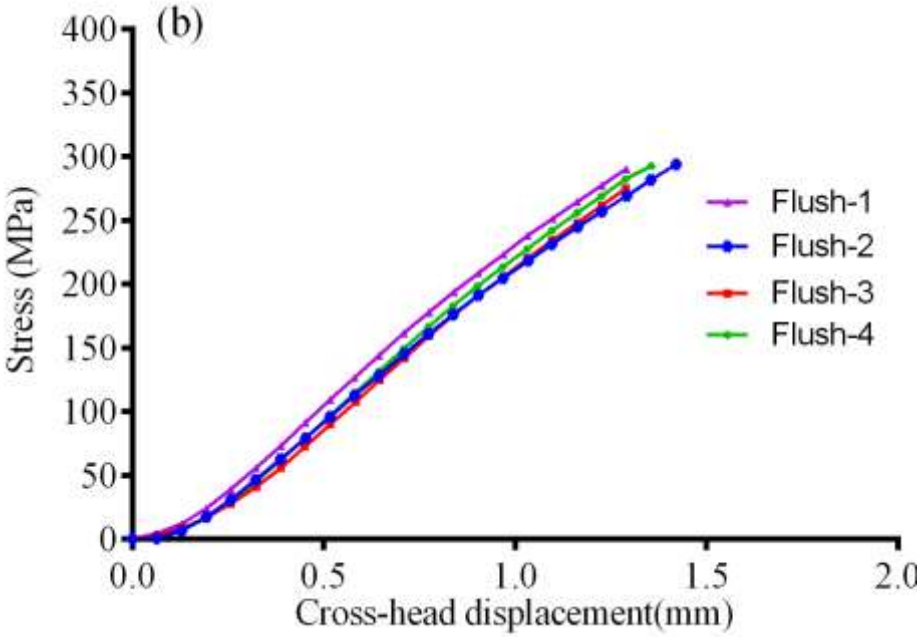

(b)

Fig. 6 Typical load-displacement curves (a) Tension (all configurations) (b) Compression (flush only)

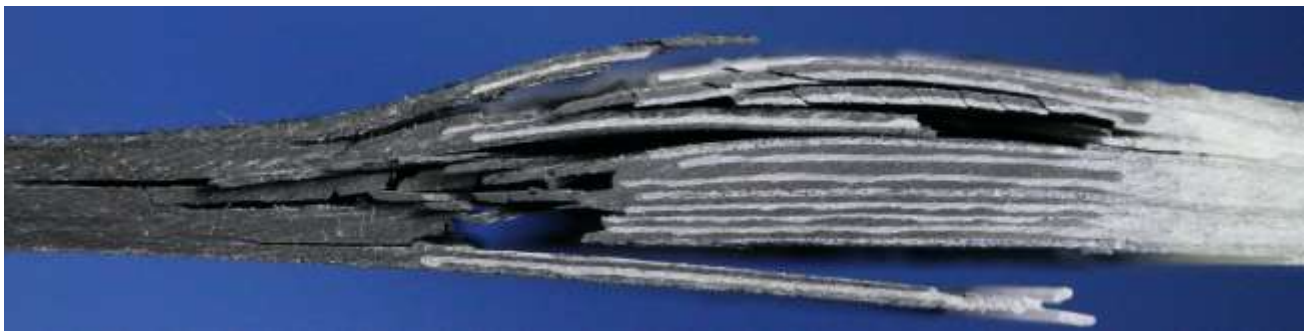

(a)

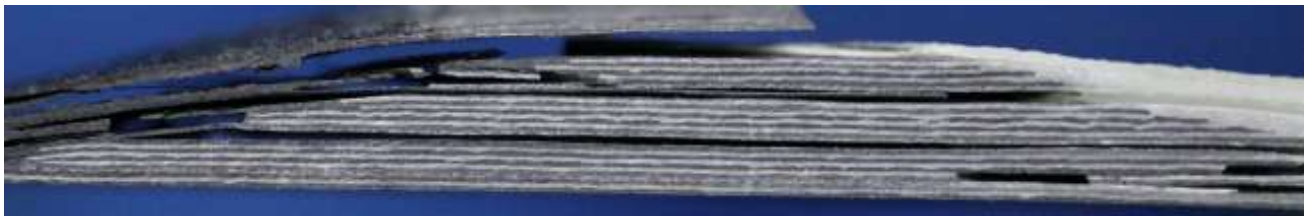

(b)

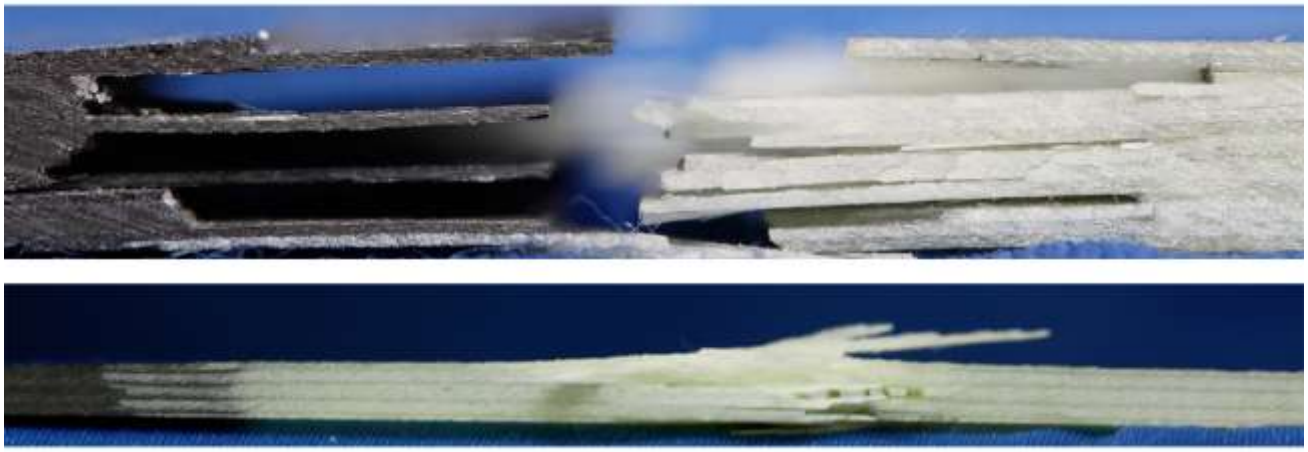

(c)

Fig. 7 Failure modes of joint specimens in tension. (a) Aligned, (b) staggered, (c-1) Flush 6 mm, and (c-2) Flush 9 mm

(a)

(b)

Fig. 8 Delaminated glass ply in Flush 6mm joint: (a) Optical image and (b) SEM image show a significant number of carbon fibres on glass ply.

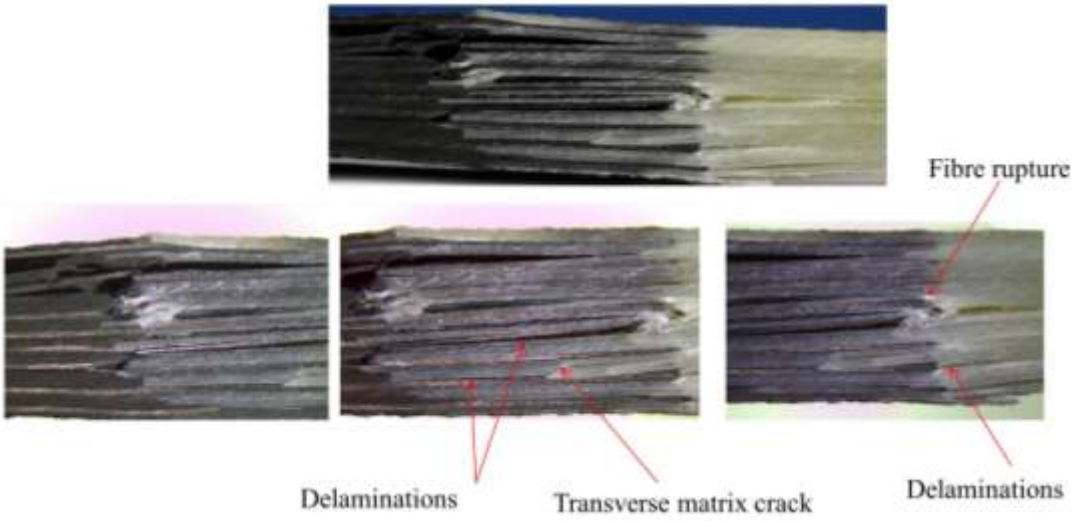

Fig. 9 Experimental failure modes of joint specimen in compression: Flush 9mm

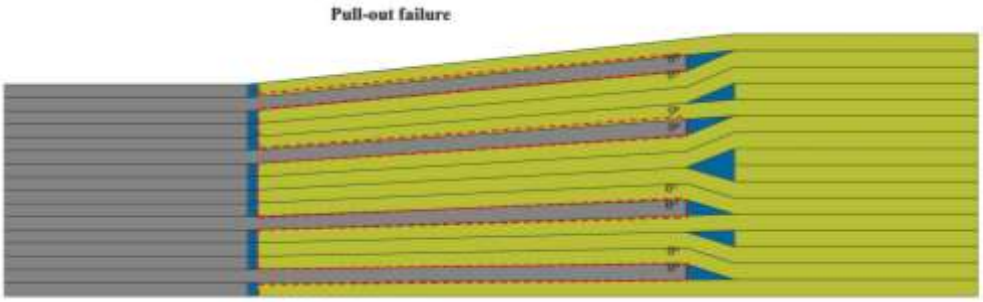
Pull-out failure

(a)

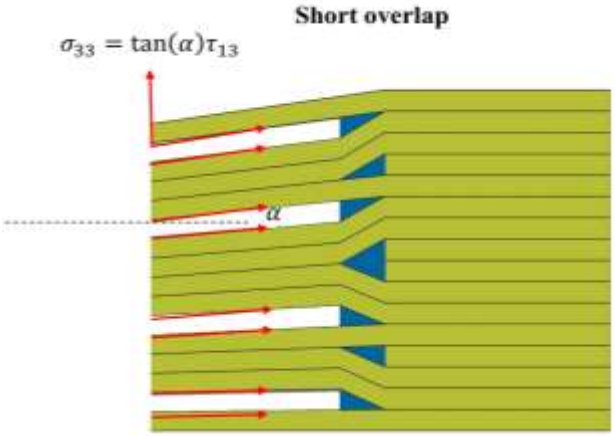
Short overlap
$\sigma_{33} = \tan(\alpha)\tau_{13}$
α

(b)

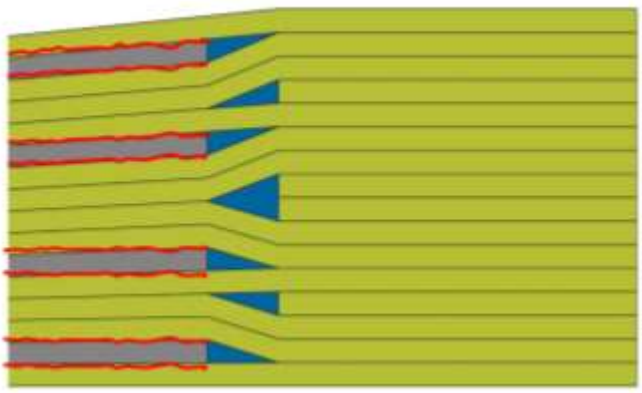
Long overlap

Fig. 10 Pull-out failure model. (a) Delamination path, (b) short overlap, and (c) long overlap

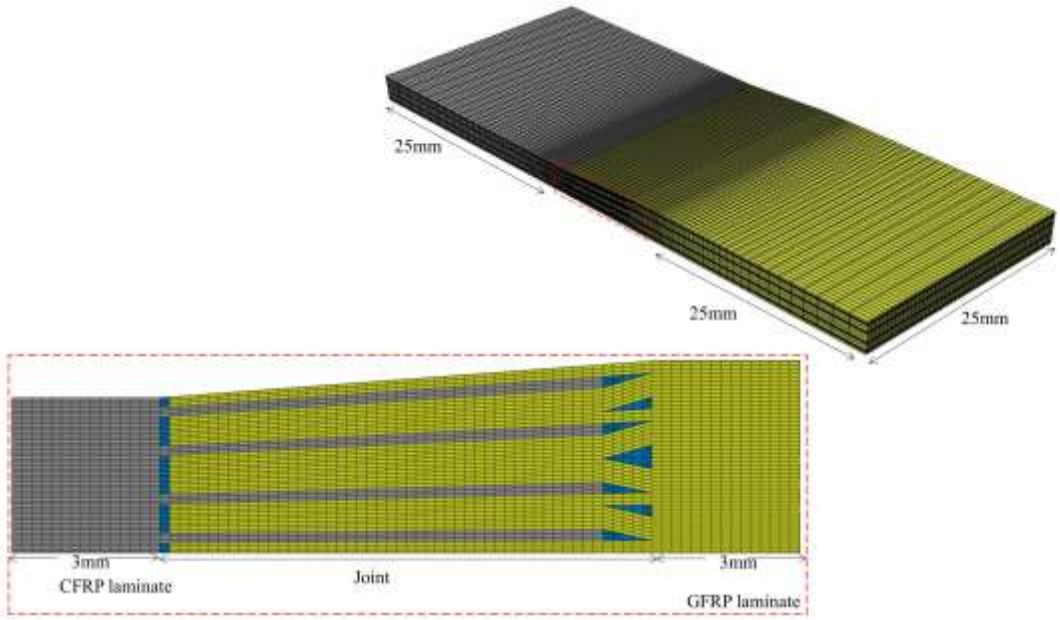

Fig. 11 Finite element model mesh of flush ply-overlap joint

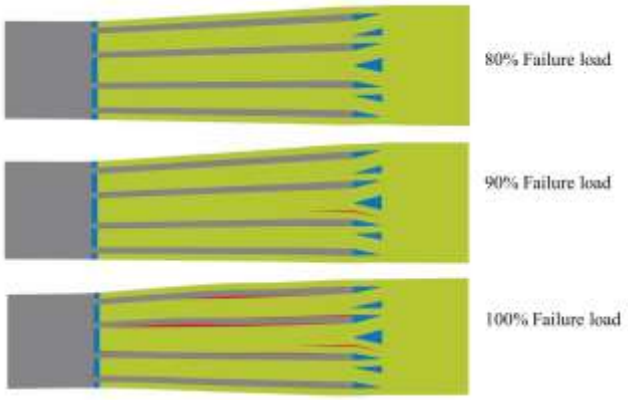

(a)

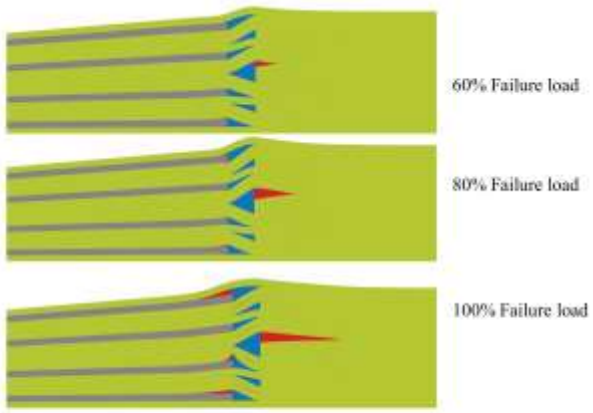

(b)

Fig. 12 FE model prediction: Damage propagation (a) Tension (b) Compression

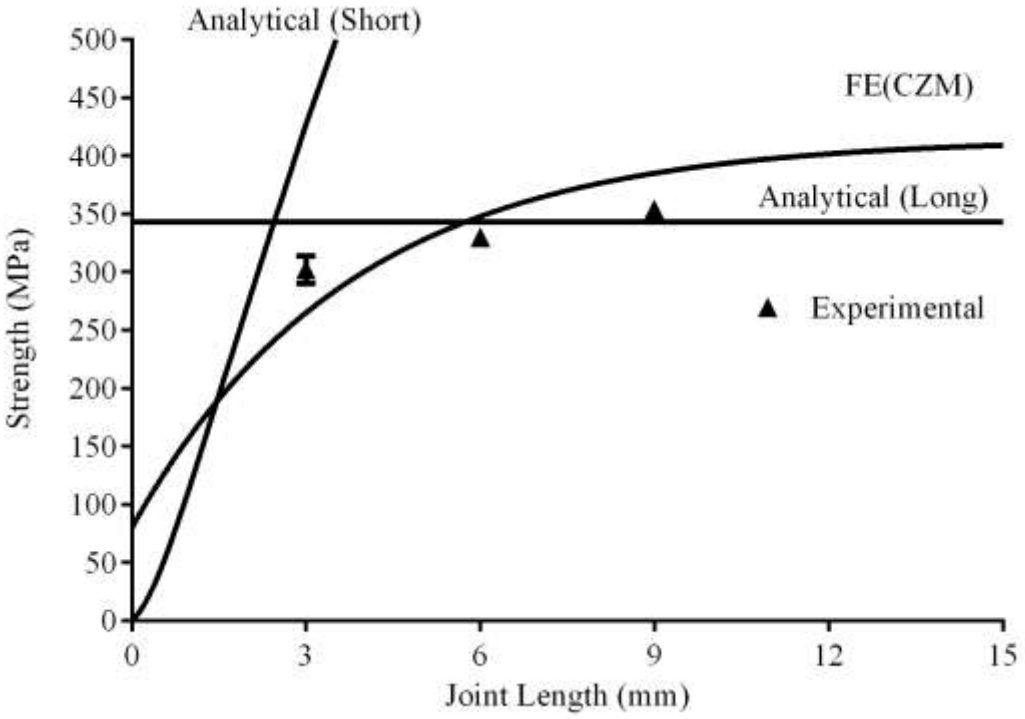
Analytical (Short)
FE(CZM)
Analytical (Long)
Experimental
Strength (MPa)
Joint Length (mm)
500
450
400
350
300
250
200
150
100
50
0
0
3
6
9
12
15

(a)

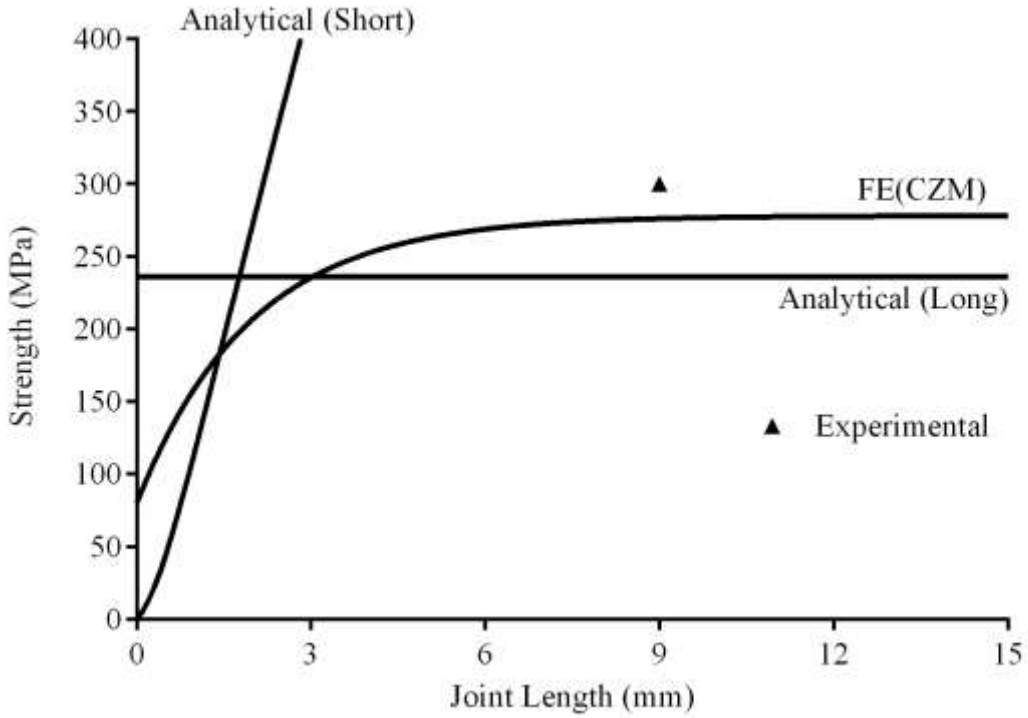

(b)

Fig. 13 Comparison of FE and analytical model predictions for the effect of overlap length on flush ply-overlap joint strength (a) Tension (b) Compression

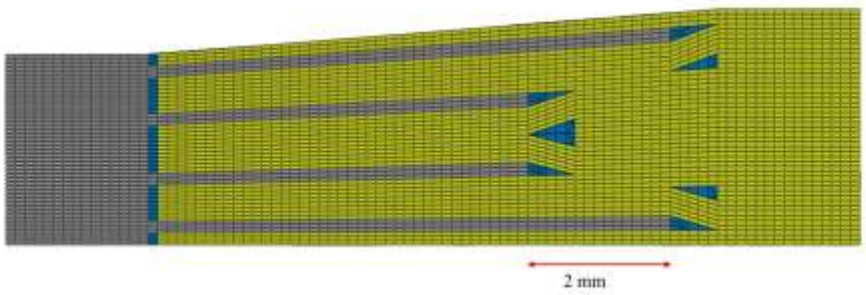

(a)

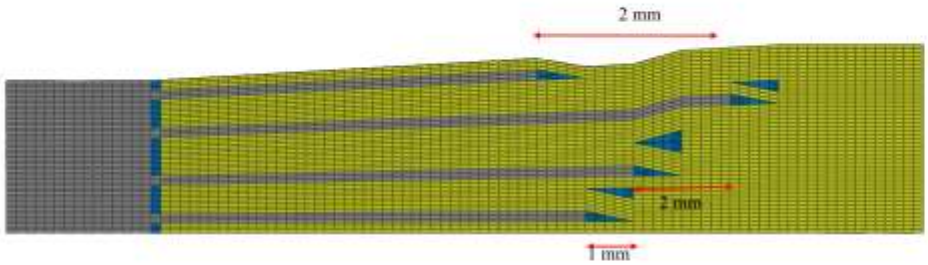

(b)

Fig. 14 Finite element models used for studying the effect of spatial distribution of ply terminations on flush ply-overlap joint strength prediction (a) Symmetric offset geometry (b) Asymmetric offset geometry (b) Note: Thermal stress not included in these predictions

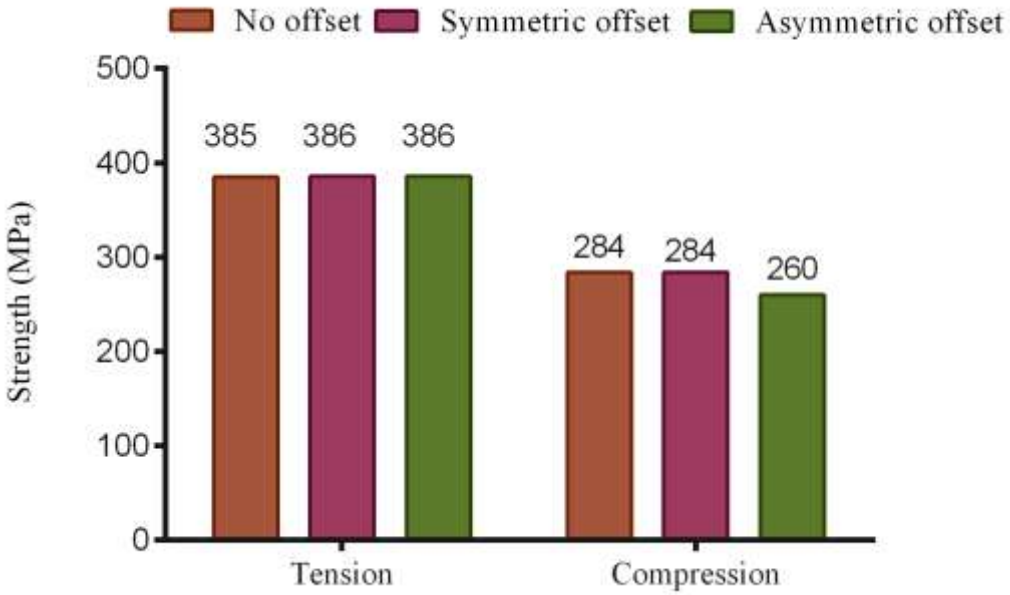

Fig. 15 Comparison of FE results for the effect of spatial distribution of ply terminations; No offset, symmetric offset and asymmetric offset